Multifrequency electron paramagnetic resonance and electron-nuclear double-resonance studies of photo-hole processes in AgBr and AgCl emulsion grains

2000 J. Phys.: Condens. Matter 12 8893

(http://iopscience.iop.org/0953-8984/12/41/316)

J. Phys.: Condens. Matter **12** (2000) 8893–8911. Printed in the UK PII: S0953-8984(00)14242-0

Multifrequency electron paramagnetic resonance and electron–nuclear double-resonance studies of photo-hole processes in AgBr and AgCl emulsion grains

R S Eachus, Th D Pawlik and R C Baetzold

Imaging Materials Division, Research and Development, Eastman Kodak Company, Rochester, NY 14650-2021, USA

Received 25 May 2000, in final form 25 July 2000

Abstract. By using a combination of multifrequency EPR spectroscopy, ENDOR spectroscopy and calculations of structure and energy, the reactivities of photo-generated holes in microcrystalline AgBr and AgCl dispersions (photographic *emulsions*) have been followed in detail. Progress has been facilitated by the use of both gelatin and polyvinyl alcohol (PVA) as peptizers. The initial trapped hole centres produced by band-gap excitation have been identified. In AgBr, this species is $[(Br_4)^{3-}\cdot V]$, a neutral complex formed from hole trapping by the four nearest neighbours of a surface Ag^+ vacancy (=V). $[(Br_4)^{3-}\cdot V]$ reacts with gelatin to produce a transient organic radical at the grain's surface. It does not, however, react with PVA. The formation of the oxidized gelatin radical might involve atomic bromine as an intermediate. In AgCl, the well-known self-trapped hole centre $(AgCl_6)^{4-}$ is the initial hole species. The hole diffuses by an electron exchange process until it is trapped by a silver ion on the grain's surface or within its penultimate layer of lattice ions. It is subsequently released from this Ag^{2+} site to be retrapped at a centre containing four equivalent Cl^- ions. The precise identity of this defect has yet to be determined, but its decay also results in the oxidation of gelatin.

1. Introduction

The behaviour of electrons produced by the photo-excitation of microscopic AgX (X = Cl, Br) grains dispersed in gelatin (photographic *emulsions*) is well understood, with much structural and dynamical information being obtained from electron magnetic resonance (EMR) experiments. A combination of cyclotron resonance [1, 2], electron paramagnetic resonance (EPR) [3], electron–nuclear double-resonance (ENDOR) [4], and optically detected magnetic resonance (ODMR) techniques [5, 6] have been used to follow the progress of electron processes from photo-generation to the formation of the latent image. EMR spectra obtained from free carriers near the conduction band edge [1, 2], electrons localized at intrinsic and impurity centres that function as shallow traps [1, 2, 7–9], and electrons deeply trapped at impurities [3, 10–12] and sensitizers [13], have all contributed to our understanding of the photographic process. In contrast, information on the behaviour of photo-holes in these materials is less complete. In AgBr grains, the photo-generated hole is believed to diffuse to the surface as a neutral (hole–Ag^+-vacancy) complex. This model was proposed to account for unexpectedly low values (i.e., 10^{-6} to 10^{-7} cm^2 s^{-1}) measured for the hole's diffusion coefficient at RT [14, 15]. In view of their low intrinsic concentration in nominally pure AgBr, the participating cation vacancies might be generated during band-gap exposure [14]. Once at the surface, the photo-holes are thought to coalesce to form molecular bromine. The driving

0953-8984/00/418893+19$30.00

force for this process is not clear. One suggestion is that the formation of Br_2 gives a ground-state wavefunction that is sufficiently localized to allow molecular desorption from the halide surface [16]. Note that none of these mechanistic and structural hypotheses are supported by direct EMR evidence, despite several of the proposed intermediates being paramagnetic.

The properties of holes in AgCl are somewhat better understood. There is compelling evidence that the initial localized photo-hole state is the self-trapped defect $(AgCl_6)^{4-}$, a tetragonally elongated molecular complex [17]. This Ag^{2+} acceptor has been detected optically by monitoring the effects of microwave radiation on donor–acceptor emission [5, 6], and by EPR spectroscopy in disordered grains and grains containing extrinsic electron traps [18]. In the latter case, recombination is suppressed by the dopants. ENDOR studies of the self-trapped hole centre have so far been frustrated by its short spin–lattice relaxation time [19]. $(AgCl_6)^{4-}$ is stable below about 40 K, but the hole diffuses at higher temperatures [20]. The fate of the hole at the grain's surface is unclear, although *molecular* chlorine evolution has been reported [21, 16].

It has been suggested that recombination events limit the speed of state-of-the-art AgX imaging materials, and that secondary-hole injection from spectrally sensitizing dye radicals causes latent image regression [13]. Thus the microscopic properties and dynamical behaviour of holes in silver halide grains, particularly at surfaces, are of technological importance as well as scientific interest. For this reason, we have completed an extensive EMR investigation of these charge carriers in microcrystalline dispersions of both AgBr and AgCl, the results of which are the basis for this report. We will compare EPR and ENDOR data obtained from pure and doped materials precipitated in gelatin and polyvinyl alcohol (PVA). The dopant selected for this study was $[Cl_5Os(NO)]^{2-}$, a deep electron trap with a small recombination cross section [22]. Incorporation of this complex increases the yield of hole centres produced by above-band-gap radiation, facilitating EMR investigations. Where appropriate, spectral assignments are confirmed by calculations of optimal defect structures and energies. A primary objective of this work is to understand hole processes at the level of detail achieved previously for electron processes.

2. Experimental issues

2.1. Materials

Several cubic AgCl dispersions in gelatin and PVA (mw = 13–23 $\times$ 10^3) were prepared for this study using standard precipitation techniques [23]. One sample was precipitated in a 50:50 mixture of PVA and sodium polyphosphate, $(NaPO_3)_n$. Grain sizes ranged between 0.05 and 0.35 μm and the dispersions were prepared with and without the addition of the diamagnetic deep electron trap $[Cl_5Os(NO)]^{2-}$. Octahedral and cubic AgBr dispersions were precipitated in gelatin and PVA. Some of these samples were doped with $[Cl_5Os(NO)]^{2-}$. The AgBr grains precipitated in gelatin ranged in size between 0.05 and 0.5 μm. In PVA, the upper size limit was about 0.11 μm. Excess peptizer was removed from each sample by a treatment involving washing with DI water at 40 °C followed by centrifugation. This was repeated three times, and then the isolated grains were rinsed with acetone, dried under N_2 at RT, and stored at 4 °C.

2.2. EPR and ENDOR measurements

Photo-EPR spectra at 9.3 GHz were measured on a Bruker ESP 300E spectrometer fitted with a helium gas-flow cryostat. *In situ* irradiations were performed with the output of a 200 W super-pressure Hg/Xe light source passing through a combination of a 1/8 m monochromator and

appropriate interference and long-pass filters. EPR measurements at 35 GHz were made with a Varian E-12 spectrometer fitted with a nitrogen gas-flow cryostat ($T = 82$–298 K). ENDOR and ENDOR-induced EPR measurements were performed on a highly modified Bruker ER 200D X-band EPR/ENDOR spectrometer described previously [24]. For ENDOR studies, the degelled dispersions were irradiated with band-gap light (365 nm) in a nitrogen gas-flow cryostat at temperatures between 82 and 210 K. These samples were then transferred via a liquid-nitrogen Dewar into the ENDOR cavity without significant warm-up. The programmes EPR-FOR [25] and SimFonia (Bruker Instruments) were used to simulate EPR spectra.

3. Results and discussion

3.1. $[Cl_5Os(NO)]^{2-}$-doped AgCl peptized in gelatin

Prior to light exposure, samples of nominally pure AgCl dispersions in gelatin frequently show EPR signals from Cu^{2+} and $Fe^{2+/3+}$ impurities. The residual peptizer in 'degelled' samples retains low levels of these ions. Fortunately these environmental impurities are unaffected by light, and so their spectra can be subtracted to reveal signals from the paramagnetic centres generated by photolysis. All of the spectra described in this report were obtained in this manner.

Figure 1(a) shows the EPR spectrum obtained from 0.1 μm AgCl cubic grains containing about 25 mppm of $[Cl_5Os(NO)]^{2-}$. It was measured at 9.3 GHz and 10 K following exposure

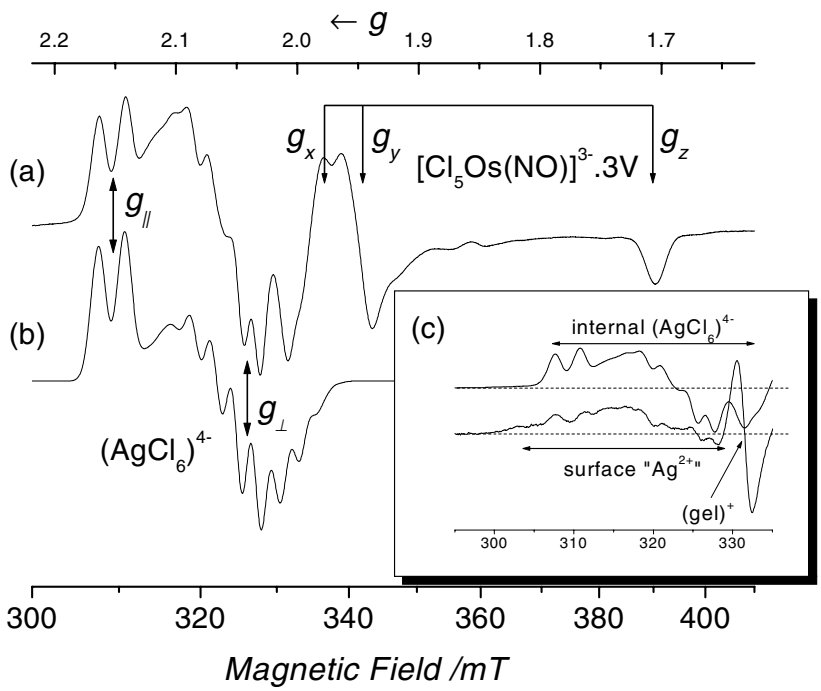

Figure 1. 9.3 GHz EPR spectra measured at 10 K from gelatin-peptized, cubic AgCl grains doped with 25 mppm $[Cl_5Os(NO)]^{2-}$. The nominal grain size was 0.1 μm. (a) Following exposure of the degelled sample to 365 nm light at 10 K. Background signals from impurities have been subtracted. (b) Simulation of the self-trapped-hole spectrum from single-crystal data. The g-factors were varied slightly to achieve an optimum fit (see the text). (c) Comparison of hole signals (upper) before annealing, and (lower) after annealing to 50 K.

of the degelled material to 365 nm light at this temperature. There are EPR signals from two photo-products. Features characteristic of the self-trapped hole centre, $(AgCl_6)^{4-}$, are evident at low magnetic field. This $4d^9$ acceptor is tetragonally elongated, the symmetry axis being defined as z [17]. Its semi-occupied molecular orbital is derived from the $4d_{x^2-y^2}$ orbital of Ag hybridized with 3s and 3p orbitals from the four equatorial Cl^- ligands. This ground state yields an axial g-matrix with $g_\parallel$ $(=g_z) > g_\perp$ $(=g_x = g_y) > 2$, as indicated in figure 1(a).

The perpendicular region of the $(AgCl_6)^{4-}$ EPR spectrum consists of superhyperfine (SHF) features from the four equivalent equatorial ligands convoluted with hyperfine (HF) lines from the central silver ion. Chlorine has two magnetic isotopes in natural abundance: ^{35}Cl ($I = 3/2$, 75.77%) and ^{37}Cl ($I = 3/2$, 24.23%). Ag also has two magnetic nuclides: ^{107}Ag ($I = \frac{1}{2}$, 51.83%) and ^{109}Ag ($I = \frac{1}{2}$, 48.17%). To first order, when the magnetic field B_0 is randomly orientated in the xy-plane, a maximum of 2508 EPR lines are expected from the ten possible combinations of chlorine and silver nuclides and their various geometrical arrangements. The large linewidths common to powder spectra obscure many of these features, leaving an 'interference pattern' of eight broad lines that is unique to $(AgCl_6)^{4-}$ in AgCl. When B_0 is parallel to z $(g_\parallel)$, the powder spectrum is further simplified. The $^{35/37}Cl$ SHF splittings are so small at this orientation that they are buried in the linewidth and only a HF doublet from the silver isotopes is resolved.

Our assignment to $(AgCl_6)^{4-}$ is based on a simulation of the powder spectrum from published single-crystal data [17]. The g-factors reported here were varied slightly from the single-crystal parameters to achieve the best spectral fit (see table 1). The resultant simulation is shown in figure 1(b). If the photo-hole is self-trapped at a lattice silver ion directly adjacent to a cation vacancy, as suggested in [20], this vacancy must be located at (002) because $(AgCl_6)^{4-}$ has axial symmetry.

Table 1. Principal magnetic resonance parameters derived for $(AgCl_6)^{4-}$ centres in AgCl. The $^{107/109}Ag$ HF and $^{35/37}Cl$ SHF splittings are reported in mT.

Location	$g_\parallel$	$g_\perp$	$\lvert A_\parallel(\mathrm{Ag})\rvert$	$\lvert A_\perp(\mathrm{Ag})\rvert$	$\lvert A'_\parallel(\mathrm{Cl})\rvert$	$\lvert A'_\perp(\mathrm{Cl})\rvert$
Bulk crystal[a]	2.1460	2.0370	3.1	2.6	2.6	0
Grain interior	2.1500	2.0400	3.1 ± 0.1	2.6 ± 0.1	2.6 ± 0.1	$\leqslant 1.0$
Grain surface	2.1320	2.0310	3.7 ± 0.1	3.0 ± 0.1	3.05 ± 0.05	$\leqslant 1.0$

[a] Taken from reference [17].

The second signal in figure 1(a) is from the deep donor centre $[Cl_5Os(NO)]^{3-}$, where the trapped electron is primarily localized on the nitrosyl ligand. The composition and geometry of this centre have been established from 9, 35 and 94 GHz EPR measurements, 9 GHz ENDOR spectra, and calculations of structure and energy [22]. Under the exposure conditions employed in this experiment, the donor is associated with silver-ion vacancies (=V) at (011), $(0\bar{1}1)$, and (002), and the Cl–Os–N=O moiety is linear. The z-direction is defined as the Cl–Os–N=O axis. The predominant $(AgCl_6)^{4-}$ trapped hole centre might also be bound to one of these vacancies, producing a neutral donor–acceptor pair with $[Cl_5Os(NO)]^{3-}$. This association of the donor and acceptor centres would be the source of the latter's slight g-factor shifts reported in table 1.

When the exposed dispersion was annealed, several important changes occurred in the EPR spectrum. (In all of the annealing experiments described in this paper, the irradiated sample was heated in the dark to the temperature specified and then quenched to 10 K in order to measure its EPR spectrum.) At about 50 K, the EPR signal from the self-trapped hole centre decreased in intensity to be replaced by a broadened signal centred at about the same field position (lower trace, figure 1(c)). A spectrum similar to this has been tentatively assigned to a

hole trapped at the AgCl–gelatin interface [24], but the structure and composition of this centre have not yet been determined. Its formation in this experiment indicates that the self-trapped hole diffuses away from the $[Cl_5Os(NO)]^{3-}\cdot 3V$ donor between 10 and 50 K. The concentration and structure of this donor, as determined by EPR, did not change as a result of hole migration. This suggests that the self-trapped hole diffuses by a process that does not involve the motion of silver-ion vacancies, i.e., through direct electron transfer between Ag^{2+} and adjacent lattice cations. The 50 K annealing treatment generated a third paramagnetic defect. It is responsible for the sharp, single line at $g = 2.0050 \pm 0.0005$ ($\Delta B = 2.0 \pm 0.1$ mT) in figure 1(c) (lower trace). Later we will assign this species as a gelatin radical formed near the AgCl grain surface by oxidation of bound peptizer residues.

For experimental reasons, our photo-ENDOR studies are currently restricted to centres produced by irradiation at $T \geqslant 77$ K. Fortunately there were few additional changes to the lower spectrum in figure 1(c) between 50 and 100 K, so an ENDOR study of the surface Ag^{2+} centre could be completed. The powder ENDOR spectrum measured at 9 K with B_0 set at 320 mT consisted of a single, broad absorption centred at 13.6 MHz, the proton Larmor frequency. This line is a matrix-ENDOR signal. Matrix-ENDOR lines result from nuclei at large distances from the paramagnetic centre so their HF interactions are only composed of the electron–nuclear dipole–dipole interaction. In general, such matrix-ENDOR lines do not provide structural information. However, if the defect is located at or near to the interface of two different materials (in this case, AgCl and gelatin), the detection of a matrix-ENDOR line from nuclides in the second matrix (gelatin) can give information about its proximity (in AgCl) to the interface region.

The intensity and shape of 'distant' ENDOR lines can be correlated with the distribution of matrix nuclei around the paramagnetic species [26]. The electron–nuclear dipole–dipole interaction is proportional to r^{-3}, where r is the separation of the electron and the nucleus in a point-dipolar approximation. The magnitude of the ENDOR effect also depends on the electron–nuclear separation ($\sim r^{-6}$). In a continuum model, the matrix-ENDOR lineshape is given by

$$f(\nu) = \int_0^{\pi} \int_a^{(q/a)^{1/3}} \frac{\cos^2\varphi \sin^3\varphi}{r^4} \left[\frac{1}{\alpha^2 + (\nu - q/r^3)} + \frac{1}{\alpha^2 + (\nu + q/r^3)} \right] \mathrm{d}r \, \mathrm{d}\varphi$$

where a defines the border between nuclei that are considered as bound to the paramagnetic defect ($r < a$) and those that are considered as matrix nuclei ($r > a$) and contribute only to the matrix-ENDOR line. The term in brackets describes an individual Lorentzian-shaped line with the linewidth α at the position given by the dipole–dipole interaction $q(\varphi)/r^3$ ($q(0) = 47.8$ MHz g_N, in atomic units). The upper limit of the integral marks the distance at which the dipole–dipole interaction becomes smaller than α, which is the limit for the ENDOR mechanism [27]. The linewidth parameter α was 80 kHz for the surface hole centre. The simulated lineshape was fitted to the experimental spectrum to obtain a best-fitted value for the mean distance a of 4.2 Å. Since the lattice constant for AgCl is about 5.55 Å at 10 K, we conclude that a substantial population of these acceptors must reside within 1–2 unit cells from the grain's surface.

The EPR spectrum of a fourth acceptor was detected following annealing to 100 K, a treatment that also increased the concentration of $(gel)^+$ radicals (figure 2(a)) and destroyed surface Ag^{2+} centres. ENDOR measurements indicated that this new acceptor was located at the AgCl grain surface, but it was not possible to analyse its EPR spectrum until a study of $[Cl_5Os(NO)]^{2-}$-doped AgBr grains was completed (see sections 3.3 and 3.4). In section 4, we will propose that this new acceptor is a $(Cl_4)^{3-}$-like defect, i.e., a hole trapped on four equivalent chloride ions, possibly associated with a surface cation vacancy.

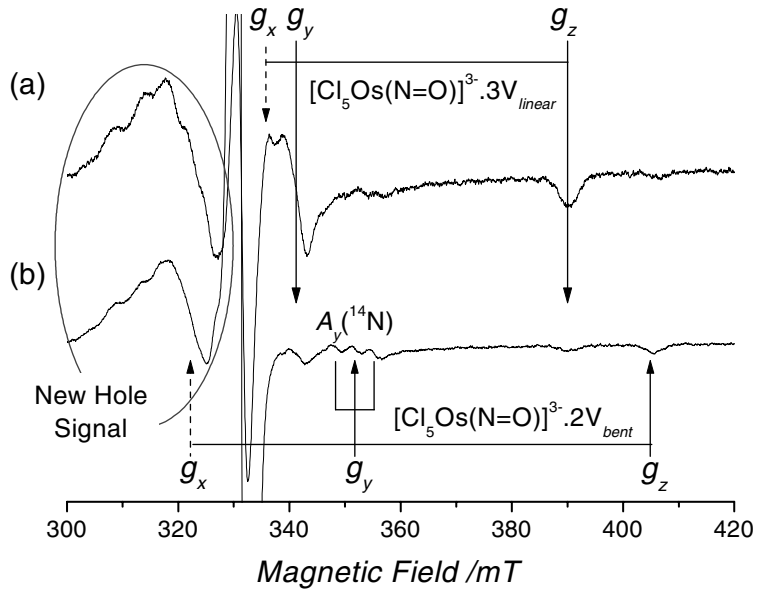

Figure 2. 9.3 GHz EPR spectra measured at 10 K from gelatin-peptized AgCl grains doped with 25 mppm $[Cl_5Os(NO)]^{2-}$. The spectra were measured after 365 nm irradiation at 10 K and warming in the dark to (a) 100 K and (b) 190 K. The strong signal at 332 mT is from the oxidized gelatin radical, $(gel)^+$. Signals from a new hole centre are observed between 300 and 320 mT.

There was a further increase in the concentration of $(gel)^+$ radicals between 100 and 190 K. Simultaneously, $\{[Cl_5Os(NO)]^{3-}\cdot 3V\}^{1-}$ underwent a structural relaxation. (The superscript outside the curly brackets refers to the net site charge in the AgCl lattice.) Previous studies have shown that this process involves the diffusion of the extra vacancy from the vicinity of the overcompensated complex to a distant lattice site or to a surface location [22]. As a result, the Cl–Os–N=O moiety bends, causing a substantial change in its EPR spectrum (see figure 2(b)). The acceptor assigned as a $(Cl_4)^{3-}$-like defect decayed at 200 K, whereas the bent $\{[Cl_5Os(NO)]^{3-}\cdot 2V\}^0$ donor and the $(gel)^+$ radical were stable for several minutes at RT.

3.2. $[Cl_5Os(NO)]^{2-}$-doped AgCl peptized in PVA

Figure 3(a) is a 9.3 GHz EPR spectrum obtained in the usual derivative mode at 10 K from 0.1 μm AgCl cubic grains precipitated in PVA solution. These grains were nominally doped with 100 mppm $[Cl_5Os(NO)]^{2-}$ and were washed and dried to remove excess peptizer. The resultant powder was exposed to 365 nm light at 10 K. EPR signals from associated $(AgCl_6)^{4-}$ acceptors and $[Cl_5Os(NO)]^{3-}$ donors are easily recognized in the figure. These centres are produced in about equal concentration. This is most obvious if we integrate the EPR spectrum, as in figure 3(b). For reference, the dashed line in this figure is the absorption spectrum of the $(AgCl_6)^{4-}$ acceptor alone, obtained from ENDOR-induced EPR experiments (see [24] and [28] for details). The areas under the donor and acceptor curves are approximately equal, indicating similar defect populations.

At 50 K, the Ag^{2+} centres migrated to the grain surface where they were stable up to at least 140 K (figure 4(a)). In PVA, there was no propensity for surface holes to react with residual peptizer. This resulted in increased stability for the Ag^{2+} acceptor. The EPR signal previously labelled $(gel)^+$ was not observed from grains peptized in PVA, this being the principal reason

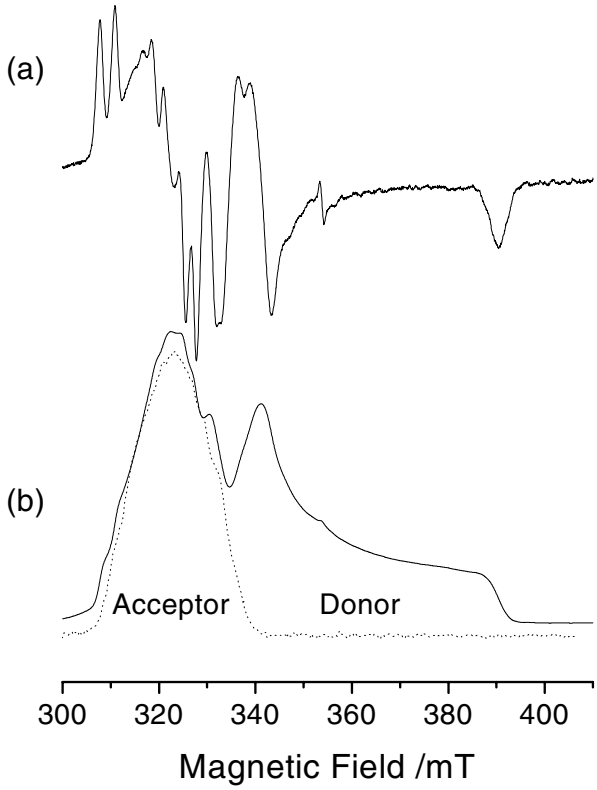

Figure 3. 9.3 GHz EPR spectra measured at 10 K from 0.1 μm AgCl cubes doped with 100 mppm $[Cl_5Os(NO)]^{2-}$. The dispersion was precipitated in PVA solution, but it was washed to remove most of the peptizer before study. The dried grains were exposed to 365 nm light at 10 K. (a) The derivative spectrum. (b) The integrated spectrum. The dashed line is the ENDOR-induced EPR signal obtained from the acceptor centre (see the text for details).

for its assignment to a gelatin radical. Figure 4(b) compares spectra from surface and internal Ag^{2+} centres, an evaluation facilitated by the absence of the $(gel)^+$ signal. The number of lines in each spectrum is the same, and both centres are uniaxial within the spectral resolution at both 9.3 GHz and 35 GHz. However, the g-factors are clearly affected by location (see table 1). In both cases, simulations show that the spectra at $g_\perp$ are composed of signals from the central silver ion and four equatorial Cl^- ligands. SHF interactions with the axial ligands are obscured by the large linewidths.

One plausible model for the surface Ag^{2+} centre is illustrated as scheme 1.

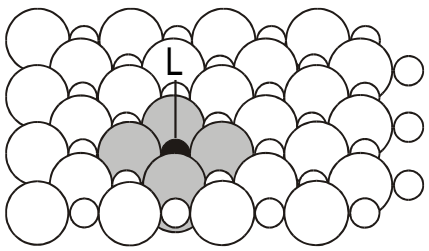

Scheme 1.

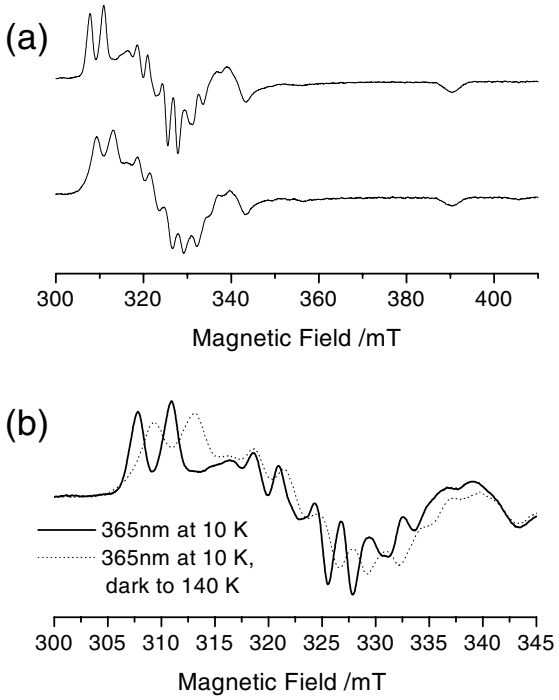

Figure 4. 9.3 GHz EPR spectra measured at 10 K from 0.1 μm AgCl cubes doped with 100 mppm $[Cl_5Os(NO)]^{2-}$. The dispersion was precipitated in PVA solution. (a) Top spectrum: from grains exposed to 365 nm light at 10 K; bottom spectrum: from grains exposed at 10 K, dark annealed to 140 K, and recooled to 10 K. (b) An expanded spectrum giving a more detailed comparison of signals from hole centres.

Here the acceptor is embedded in the grain surface and the equatorial chloride ligand shell is intact. It is logical that the fifth ligand, located in the penultimate layer, is also Cl^-. Neither EPR nor ENDOR spectroscopy helped identify L, a sixth ligand included to satisfy the propensity of Ag^{2+} for octahedral coordination. It could be chloride, or a species derived from the grain's environment during precipitation such as NO_3^-, or H_2O.

An alternative model has the Ag^{2+} ion located subsurface, perhaps in the penultimate crystal plane, so that it retains a full chloride ligand shell, as in scheme 2.

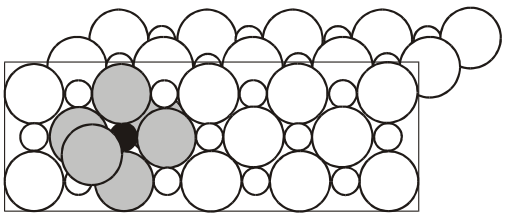

Scheme 2.

ENDOR measurements have so far failed to resolve this issue, because, as for gelatin, only matrix signals were observed from the PVA-peptized materials.

One experiment provided further confirmation that the matrix-ENDOR lines are indeed due to electron–nuclear dipole–dipole interactions between an Ag^{2+} centre located at the surface of the AgCl grain and magnetic nuclides in the peptizer. An $[Cl_5Os(NO)]^{2-}$-doped AgCl

dispersion was prepared in a 50:50 mixture of PVA and sodium polyphosphate. In this mixed peptizer, the ENDOR spectrum of the high-temperature Ag^{2+} species has two features in the region between 5 and 25 MHz (figure 5). As for pure PVA, the most prominent is a matrix-ENDOR line centred at the proton Larmor frequency (13.95 MHz at $B_0 = 326.7$ mT). In the presence of polyphosphate, an additional weaker signal is found at 5.65 MHz, the Larmor frequency of ^{31}P at this field position.

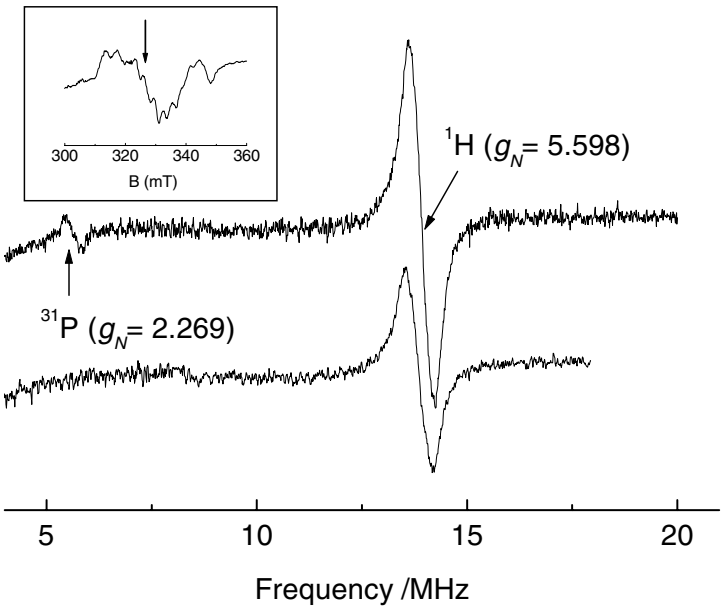

Figure 5. 9.3 GHz powder ENDOR spectra obtained at 10 K from $(AgCl_6)^{4-}$ centres in $[Cl_5Os(NO)]^{2-}$-doped AgCl grains. Samples were exposed to 365 nm light at 90 K. Spectra were measured with $B_0 = 326.7$ mT, the field position indicated by the arrow in the inset EPR spectrum. Upper ENDOR spectrum: grains precipitated in PVA/$(NaPO_3)_n$ solution. Lower ENDOR spectrum: grains precipitated in PVA solution.

Annealing at temperatures between 160 and 190 K caused the surface Ag^{2+} centres to decay. As a result, a strong EPR signal from the species identified as a $(Cl_4)^{3-}$-like acceptor was revealed. Heating above 200 K destroyed this centre, but without producing the PVA analogue of the gelatin radical cation.

3.3. $[Cl_5Os(NO)]^{2-}$-doped AgBr peptized in gelatin

Figure 6 includes 9.3 GHz EPR spectra obtained at 10 K from a sample of an $[Cl_5Os(NO)]^{2-}$-doped AgBr dispersion that was precipitated in gelatin. The grains were 0.5 μm octahedra doped homogeneously with 25 mppm of this electron trap, and most of the peptizer was removed by degelling. A spectrum obtained prior to irradiation showed the grains to be essentially free of paramagnetic impurities. Figure 6(a) was measured following exposure to 440 nm light at 10 K. Three paramagnetic species were generated by this band-to-band excitation, one of which is in low concentration and is thought to be $[Cl_4BrOs(NO)]^{3-}$ formed by electron trapping at a dopant contaminant. The majority of centres give rise to the relatively well-resolved signal in the region between 325 and 425 mT, and the broad, asymmetric feature near 315 mT. The first signal is very similar to that assigned to $[Cl_5Os(NO)]^{3-}$ donors in

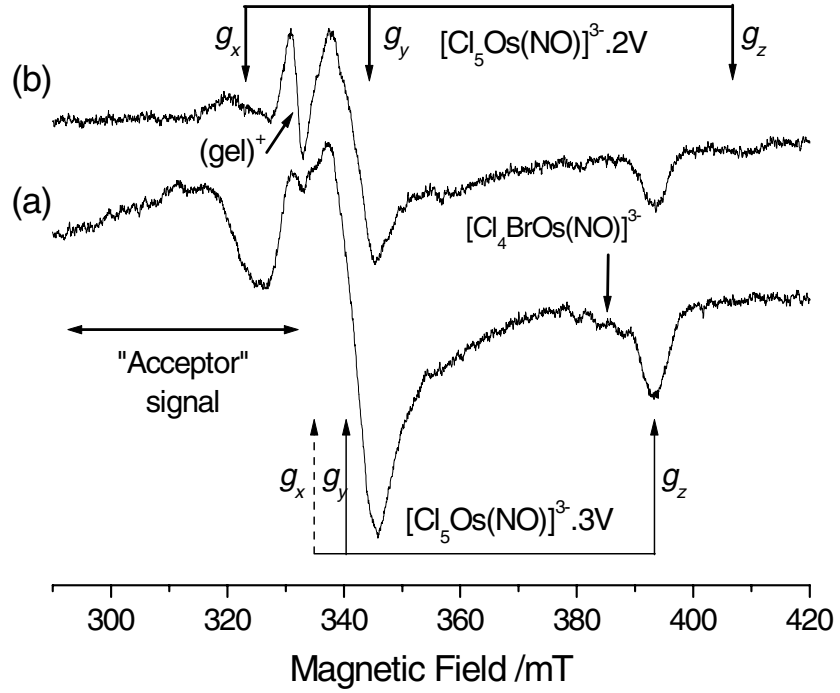

Figure 6. 9.3 GHz EPR spectra measured at 10 K from an $[Cl_5Os(NO)]^{2-}$-doped AgBr dispersion in gelatin. The grains were 0.5 μm octahedra. Samples were exposed to 440 nm light at (a) 10 K and (b) 150 K. The weaker signals at 380–395 mT in (a) are tentatively assigned as an HF quartet from $^{79/81}$Br nuclides in a $[Cl_4BrOs(NO)]^{3-}$ impurity centre.

AgCl, an opinion supported by the magnetic resonance parameters included in table 2 and a comparison of figures 6(a) and 1(a). Thus, by analogy, the $[Cl_5Os(NO)]^{3-}$ centre formed by exposure at 10 K in AgBr is assumed to be associated with Ag^+ vacancies at (011), $(0\bar{1}1)$ and (002), and the Cl–Os–N=O moiety is linear. This is consistent with calculations of structure and energy.

Table 2. Principal magnetic resonance data for the $[Cl_5Os(NO)]^{3-}\cdot 3V$ donor in AgBr and AgCl. The ^{14}N HF data are quoted in mT.

Lattice	g_x	g_y	g_z	$\lvert A_x\rvert$	$\lvert A_y\rvert$	$\lvert A_z\rvert$
AgCl[a]	1.9980	1.9487	1.7030	3.28	1.34	$\leqslant 1$
AgBr	1.9926	1.9430	1.6923	3.0	—[b]	—[b]

[a] Taken from reference [22].
[b] Values not determined experimentally due to the large spectral linewidth.

Because the photo-physics of nominally pure AgBr grains at 10 K is dominated by recombination, a corollary to the production of $[Cl_5Os(NO)]^{3-}$ donors must be the formation of acceptors in equal concentration. For this reason, we assign the low-field spectrum in figure 6(a) to a photo-generated hole centre. This centre is invariably detected in EPR studies of shallow and deep electron trapping dopants in AgBr. It is also commonly observed in optically detected magnetic resonance experiments on nominally pure samples of this material [6]. Unfortunately, the absence of clear HF or SHF features in the EPR and ODMR spectra

precludes the derivation of a specific structural model. The EPR signal overlaps that from copper contaminants in the peptizer, but, in our experience, Cu^{2+} coordinated to gelatin is not affected by 440 nm light. Furthermore, the quartet of lines at $g_{\parallel}$ characteristic of cupric ions, which result from HF interactions with the magnetic ^{63}Cu and ^{65}Cu nuclides, is not resolved here. We attribute the signal at about 317 mT to an *intrinsic* acceptor and will later substantiate this assignment with data obtained from AgBr dispersions in PVA (section 3.4). We will also derive its composition and structure in section 4.

When the $[Cl_5Os(NO)]^{2-}$-doped AgBr grains were exposed to 440 nm light at 10 K, annealed in the dark, and then quenched to 10 K, the EPR spectrum changed predictably. Around 130 K, the $[Cl_5Os(NO)]^{3-}\cdot 3V$ donor centre relaxed to the more stable $[Cl_5Os(NO)]^{3-}\cdot 2V$ configuration. A signal from this complex can just be discerned in figure 6(b). By analogy to the results from AgCl [22], we assume that the extra Ag^+ vacancy at (002) migrates to the grain's surface during this annealing treatment, and that the resultant crowding causes the Cl–Os–N=O moiety to bend. At about 160 K, the spectrum of the intrinsic hole centre narrowed significantly before it reacted completely with residual peptizer to generate $(gel)^+$. This peptizer radical produced a single EPR line at $g = 2.0056 \pm 0.0005$. The structure of the intermediate hole centre responsible for the narrowed EPR signal, labelled here as i_{Br}, has not been determined experimentally. By 250 K, both the relaxed osmium donor and the $(gel)^+$ radical had decayed.

3.4. $[Cl_5Os(NO)]^{2-}$-doped AgBr peptized in PVA

The 9.3 GHz EPR spectrum shown in figure 7(a) was obtained at 10 K from an $[Cl_5Os(NO)]^{2-}$-doped AgBr dispersion in PVA following its irradiation with 440 nm light. The nominal grain size was 0.1 μm and the dopant concentration was about 100 mppm. The donor spectrum extending from about 330 mT to 400 mT can be assigned to the linear, overcompensated complex $[Cl_5Os(NO)]^{3-}\cdot 3V$, following the arguments in section 3.3. The corresponding hole centre spectrum, which is broad and featureless for grains in gelatin, is clearly resolved for this PVA-peptized dispersion. An interpretation of this spectrum has been achieved by combining the 9.3 GHz EPR data with the results of EPR studies at 35.4 GHz, and ENDOR and ENDOR-induced EPR experiments at 9.1 GHz.

The 9.3 GHz EPR spectrum was analysed assuming a paramagnetic centre with $S = \frac{1}{2}$ and uniaxial symmetry. In order to assess the validity of our analysis, powder spectra were simulated to second order. The best fit (figure 7(b)) was achieved with $g_1 = g_{\parallel} = 2.0800 \pm 0.001$ and $g_2 = g_3 = g_{\perp} = 2.0640 \pm 0.001$. The features centred at $g_{\perp}$ are split into septets with intensity distributions of 1:2:3:4:3:2:1, line separations of 12.8 ± 0.5 mT, and peak-to-peak linewidths of about 11.7 mT. The last three features of these septets are obscured by overlap with the osmium donor spectrum. Measuring the EPR spectrum at 35.4 GHz (figure 7(c)) reveals two of these high-field lines. The feature at $g_{\parallel}$ with a linewidth of about 5.5 mT shows no HF or SHF structure at either microwave frequency. A 35.4 GHz spectrum simulated from the 9.3 GHz data (figure 7(d)) was consistent with the results of the high-frequency experiment, providing support for this analysis. Fitting required only a slight increase in the spectral linewidth, possibly the result of lower B_0-field homogeneity combined with g-strain broadening at the higher microwave frequency.

We attempted to obtain additional HF and SHF information by measuring ENDOR spectra at B_0-positions within the envelope of this hole centre's EPR signal. At all field values between 280 and 325 mT, the ENDOR spectrum comprised a single, intense line centred at the ^1H Larmor frequency. This matrix-ENDOR line originates from electron–nuclear dipole–dipole interactions between the hole centre in/on AgBr and protons in PVA and/or water at the

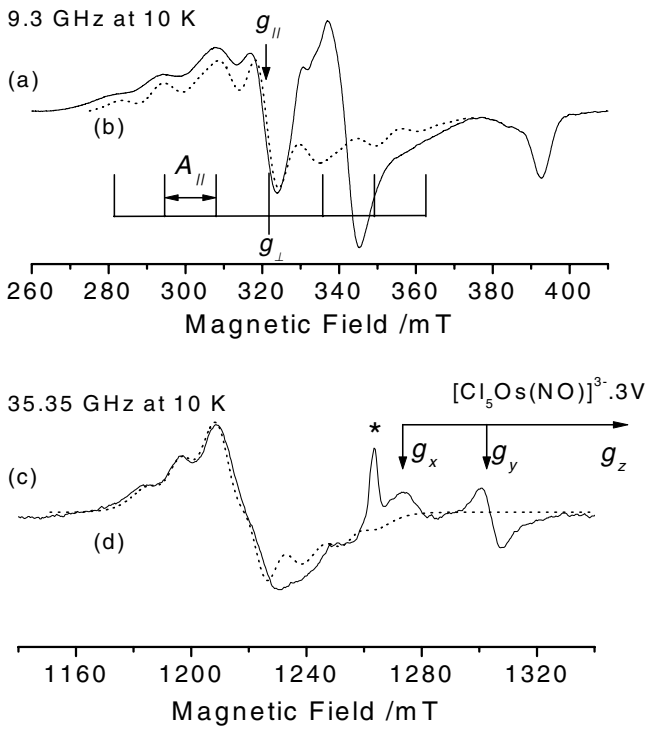

Figure 7. EPR spectra obtained at 10 K from 0.1 μm AgBr octahedra in PVA. The dispersion was doped with 100 mppm $[Cl_5Os(NO)]^{2-}$ and was irradiated with 440 nm light at (a) 10 K and (c) 82.5 K. Spectra were measured at (a) 9.3 GHz and (c) 35.4 GHz. Dashed line (b) is spectrum fitted to experimental data based on the $(Br_4)^{3-}\cdot V$ model discussed in the text. The dashed line (d) was computed from the 9.3 GHz data allowing for a 15% increase in the peak-to-peak linewidth. The feature marked $*$ is from a cavity resonance.

grain's surface, and its intensity was sufficient to perform an ENDOR-induced EPR (EI-EPR) experiment. The EI-EPR signal is, in effect, the analogue of an excitation spectrum obtained in luminescence experiments. It is the EPR spectrum of the species responsible for the matrix-ENDOR signal, isolated from all other features in the conventionally detected EPR spectrum. Figure 8 is the EI-EPR spectrum of the hole centre, obtained in absorption mode, plotted with the integral of the experimental data from figure 7(a) and the integral of the spectrum simulated for the hole centre. The EI-EPR spectrum is a broad, almost symmetric absorption centred at about 320 mT. Clearly the high-field wing of this signal overlies much of the field region corresponding to the EPR spectrum from $\{[Cl_5Os(NO)]^{3-}\cdot 3V\}^{1-}$, as assumed in our analysis of figure 7(a).

The formation of this hole centre is not restricted to AgBr grains containing $[Cl_5Os(NO)]^{2-}$. Figure 9 compares the spectrum obtained from the 0.1 μm, $[Cl_5Os(NO)]^{2-}$-doped material (from figure 7(a)) with that obtained from a nominally pure, 0.1 μm octahedral dispersion in PVA. Both spectra were measured at 10 K following 440 nm irradiation and each contains the distinctive features that we assign to the intrinsic hole centre. For reference, we performed the same photolysis experiment on a dispersion of undoped 0.5 μm AgBr octahedra prepared in gelatin solution. In this case the yield of paramagnetic centres was small in the absence of a deep electron trap, but the hole's EPR signal could be resolved at high signal amplification (figure 9(c)).

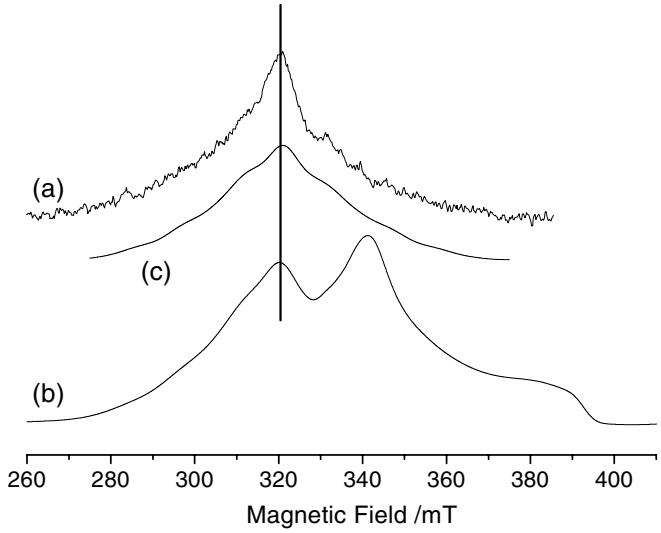

Figure 8. (a) An ENDOR-induced EPR spectrum obtained from the ^{1}H matrix-ENDOR signal from 0.1 μm AgBr octahedra in PVA. The dispersion was doped with 100 mppm $[Cl_5Os(NO)]^{2-}$ and was irradiated with 440 nm light at 82.5 K. (b) The integral of the EPR spectrum shown in figure 7(a). (c) The integral of the spectrum simulated for $(Br_4)^{3-}\cdot V$ in AgBr.

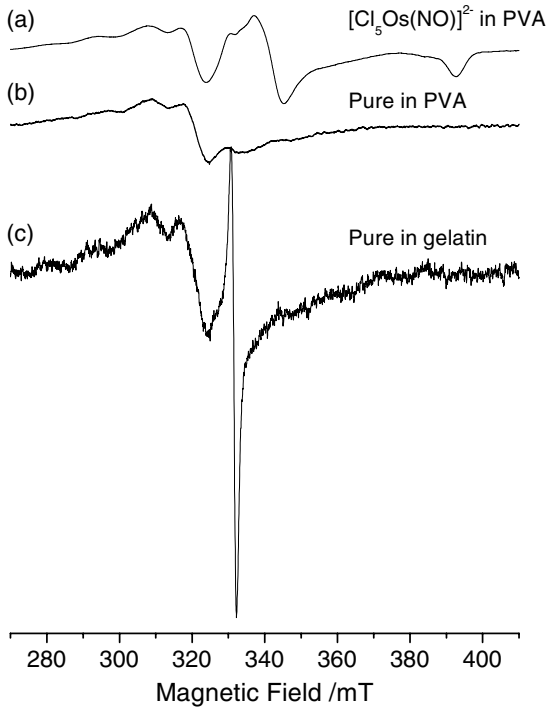

Figure 9. 9.3 GHz EPR spectra measured at 10 K from (a) 0.1 μm AgBr octahedra containing 100 mppm $[Cl_5Os(NO)]^{2-}$ and dispersed in PVA, (b) pure 0.1 μm AgBr octahedra dispersed in PVA, and (c) pure 0.5 μm AgBr octahedra dispersed in gelatin. (a) and (b) were measured after 440 nm exposure at 10 K. (c) was obtained following 440 nm at 120 K. The strong, single line in (c) is from $(gel)^{+}$.

4. Structural assignments

There are sufficient magnetic resonance data available to permit the development of a structural model for the intrinsic hole centre in AgBr grains. The 1:2:3:4:3:2:1 intensity distribution of the features comprising the septet at g_1 in figure 7(a) shows that they result from the interaction of the unpaired electron with two equivalent nuclei of spin $I = 3/2$. The most common $I = 3/2$ nuclei are ^{7}Li, ^{11}B, ^{23}Na, ^{35}Cl, ^{37}Cl, ^{39}K, ^{53}Cr, ^{63}Cu, ^{65}Cu, ^{79}Br, and ^{81}Br. The bromine nuclides are the most likely source of these septet splittings in AgBr. The 11.7 mT linewidth prevents the resolution of the individual ^{79}Br (50.69%) and ^{81}Br (49.41%) contributions. A model similar to that of the V_K centre in alkali halides is immediately suggested [29], where two equivalent bromide ions, labelled Br_1 and Br_2 in scheme 3, equally share the trapped hole.

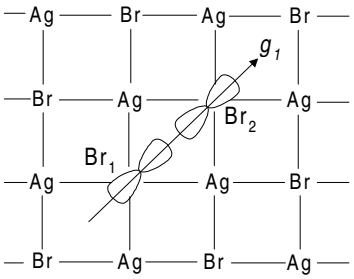

Scheme 3.

The hole occupies an anti-bonding molecular orbital formed across the diagonal of the unit cell. The loss of an anti-bonding electron strengthens the interaction between Br_1 and Br_2 and causes them to relax in the manner shown. In KBr, the bare V_K centre has close to uniaxial symmetry ($g_1 = 1.980$, $g_2 = 2.179$, $g_3 = 2.175$, $A_1 = 45.5$ mT, and $A_2 = A_3 = 8.0$ mT) and its principal axis is orientated along [110]. In this situation, we expect a large septet HF splitting (=45.5 mT) when B_0 is along g_1 ($\equiv g_\parallel$). In the $g_\perp$-plane ($g_\perp \equiv g_1 \approx g_2$), seven HF lines are expected at each orientation of B_0, but the splitting will be much smaller (=8.0 mT). We have simulated the powder EPR spectrum expected for a V_K-like hole centre in AgBr, using our experimental magnetic resonance parameters. The result, shown in figure 10(a),

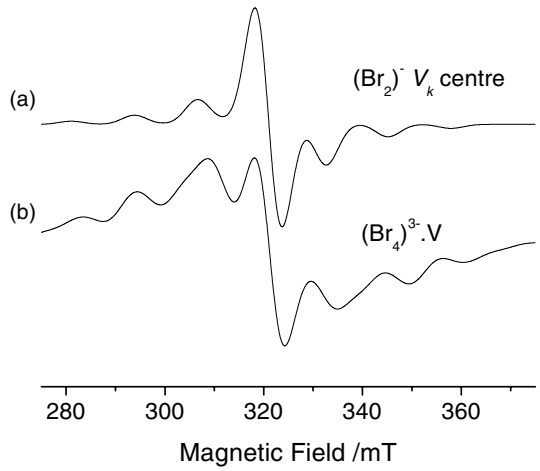

Figure 10. 9.3 GHz EPR spectra simulated for (a) a Br_2^- V_K-like centre, and (b) the $(Br_4)^{3-}\cdot V$ centre in AgBr. The experimental HF parameters and g-factors were used in these simulations.

resembles the 9.3 GHz EPR spectrum in figure 7(a), but there is one crucial difference. In the simulation, the resolved septet of features centred at $g_\parallel$ is noticeably weaker than the signal at $g_\perp$. This is a consequence of statistics. There are considerably more orientations close to, and within the plane containing g_2 and g_3 than orientations close to the unique direction of g_1. In contrast, the experimental spectrum shows the septet to be significantly more intense than the central derivative-like feature. An additional argument against an assignment to $(Br_2)^-$ in AgBr is that the largest HF splitting is only 12.8 mT compared to the value of 45.5 mT reported for this centre in KBr [29].

We believe that the spectra in figure 7 can be better explained by scheme 4, where the trapped hole is in a ground-state molecular orbital derived from bromine $4p_x$ and $4p_y$ atomic orbitals.

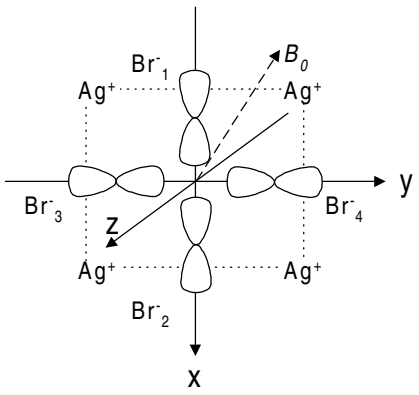

Scheme 4.

From symmetry, $g_x = g_y = g_\perp$ and $g_z = g_\parallel$. When the applied magnetic field B_0 is parallel to x, the EPR spectrum consists of seven lines split by $A_\parallel$ from HF interactions with Br_1 and Br_2. To first order, each of these lines should be further split into a septet separated by $A_\perp$ from HF interactions with Br_3 and Br_4. However, $A_\perp$ is too small to be resolved from the large linewidths of the 9.3 and 35 GHz spectra. From simulations, we set an approximate upper limit of 0.9 mT for $A_\perp$. An identical spectrum would be observed with B_0 aligned along y, with the largest HF interaction now resulting from Br_3 and Br_4. When B_0 is parallel to z, the spectrum would consist of 13 lines split by $A_\perp$ from HF interactions with the four equivalent Br nuclides, but these features are also obscured by the large spectral linewidth. The result is a single broad feature centred at $g_\parallel$. Because the HF lines separated by $A_\parallel$ are now centred at $g_\perp$, the absorption-like parallel features in the powder spectrum are statistically enhanced in intensity relative to the derivative signal at $g_\parallel$. The simulated spectrum, shown in figures 7(a) and 10(b), was computed on this basis. From these arguments, the intrinsic hole centre produced by above-band-gap irradiation at 10 K is assigned as a $(Br_4)^{3-}$ centre located at, or near to, the grain's surface.

It is possible to estimate the distribution of the unpaired electron between the four bromide ions in $(Br_4)^{3-}$ from the HF data. Because the signs of $A_\parallel$ and $A_\perp$ are not known, we must consider all possible combinations, as in table 3. The usual relationships $A_\parallel = A_{iso} + 2b$ and $A_\perp = A_{iso} - b$ hold, where A_{iso} and b are related to the contributions of s and p orbitals, respectively, to the ground-state wavefunction. A_{iso} can be used to estimate the s-orbital contribution from each ion, σ_s, by comparing the experimental value to that calculated for unit occupancy of the 4s orbital. Likewise b can be used to estimate the 4p-orbital contribution, σ_p. Because the individual ^{79}Br and ^{81}Br HF data were not resolved experimentally, we have used averaged values for the theoretical parameters taken from table G.4 of reference [30]. Two

Table 3. Analyses of magnetic resonance parameters for $(Br_4)^{3-}\cdot V$ in AgBr and $(Br_2)^-$ in KBr [29] carried out to obtain spin densities. HF values are quoted in mT.

	$(Br_4)^{3-}\cdot V$ in AgBr				$(Br_2)^-$ in KBr			
$A_\parallel$	12.8	12.8	−12.8	−12.8	45.5	45.5	−45.5	−45.5
$A_\perp$	0.9	−0.9	0.9	−0.9	8.0	−8.0	−8.0	8.0
A_{iso}	4.88	3.67	−3.67	−4.88	20.5	9.83	−20.5	−9.83
$2b$	7.93	9.13	−9.13	−7.93	25.0	35.67	−25.0	−35.67
$-b$	−3.97	−4.57	4.57	3.97	−12.5	−17.83	12.5	17.83
σ_s	0.004	0.003	−0.003	−0.004	0.017	0.008	−0.017	−0.008
σ_p	0.131	0.151	−0.151	−0.131	0.412	0.588	−0.412	−0.588
$\lambda = \sigma_p/\sigma_s$	32.75	50.33	50.33	32.75	24.24	73.5	24.24	73.5
$\sigma_s + \sigma_p$	0.135	0.154	−0.154	−0.135	0.429	0.596	−0.429	−0.596
Total	0.540	0.616	−0.616	−0.540	0.858	1.192	−0.858	−1.192

sign combinations give reasonable (i.e., positive) values for σ_s and σ_p, and appropriately large values for the hybridization ratio (λ). However, both combinations fail to account for 40–50% of the unpaired electron density. For comparison, a similar analysis has been performed for the $(Br_2)^-$ V_K centre in KBr [29]. Only one sign combination (all positive) gives physically meaningful results, with over 85% of the electron density shared between the two bromide ions. We can rationalize these results if we propose that, in AgBr, overlap between the 4p orbitals of the four bromide ions is mitigated by a central silver-ion vacancy. Because a cation vacancy carries an effective charge of −1, the resultant centre, $(Br_4)^{3-}\cdot V$, is electrically neutral.

To assess the viability of the proposed model, its energy, optimum structure, and unpaired electron distribution were addressed theoretically. These calculations involved procedures developed for intrinsic defects on silver halide surfaces [31]. We constructed an $Ag_{13}Br_{17}$ quantum mechanical model embedded in the flat surface of a hemispherical array of point charges arranged at Ag^+ and Br^- sites and having an overall neutral charge. In this model, twenty quantum mechanical ions were arranged in the top surface around a central silver-ion vacancy. A second plane contained nine quantum mechanical ions and a third contained one, all symmetrically positioned around the vacancy. Both unrestricted Hartree–Fock (UHF) and density functional (DFT) calculations were performed on this model. The halide and silver ions nearest to the vacancy were allowed to relax while the other ions were kept fixed. We studied the composition of the resulting wavefunction for a double-zeta basis set having two basis functions per orbital and corresponding pseudopotentials [32, 33], as in prior work [4, 18, 22, 24]. The wavefunction was analysed by means of a Mulliken analysis to give unpaired electron densities on the ions treated quantum mechanically. In both the DFT and UHF calculations, we found that the predominant spin density is on the four bromide ions next to the Ag^+ vacancy, and at least 99% of the spin density is on ions in the surface plane. Since the UHF calculations contained no correlation energy effects, we consider the DFT results to be more realistic. The DFT calculation gave calculated spin populations of 0.146 on each of the four bromide ions sharing the surface vacancy, 0.053 on each of the four nearest-neighbour Ag^+ ions, and 0.024 on the eight Br^- ions at next-nearest-neighbour positions in the AgBr surface. We also examined several other basis sets, but the spin populations obtained were within 5% of those quoted above. These results support the surface nature proposed for this trapped hole centre, and the calculated spin densities are in reasonable agreement with experiment for the combinations with $A_\parallel$ and $A_\perp$ positive or $A_\parallel$ positive and $A_\perp$ negative (table 3). We take this

correlation between experiment and theory as substantial support for the $(Br_4)^{3-}\cdot V$ model.

We now turn to the identity of the species formed in AgCl from the decay of the surface Ag^{2+} centre. Its spectrum is shown in figure 11(a). Prompted by the results obtained for AgBr, we have attempted to analyse this spectrum in terms of a $(Cl_4)^{3-}\cdot V$ model. We achieved a reasonable fit to the experimental spectrum from a simulation based upon the following parameters: $g_\parallel = 2.063 \pm 0.005$, $g_\perp = 2.059 \pm 0.002$, $A_\parallel = 4.2 \pm 0.5$ mT, and $A_\perp = 0.5 \pm 0.3$ mT. The estimated errors are large because of the considerable experimental linewidths ($\Delta B_\parallel = 9.0$ mT, $\Delta B_\perp = 2.5$ mT). Once again, $A_\parallel$ is derived from the septet of HF features centred at $g_\perp$, and $A_\perp$ is estimated from fitting a broad feature at $g_\parallel$. The simulated spectrum is shown in figure 11(b). There are small differences in the region around $B_0 \approx 324$ mT, and at the high-field edge, but the simulation reproduces the majority of the experimental features. The comparison is confused slightly by the superposition of a weak signal from oxidized gelatin radicals at about $B_0 = 332$ mT. Broadening in the wings, especially at high field, could be the result of $^{35}Cl/^{37}Cl$ isotope effects (neglected in our analysis) combined with second-order field effects. This result supports an assignment to $(Cl_4)^{3-}\cdot V$, but a spin-population analysis of the HF data reveals some inconsistencies. We followed the procedure outlined above for $(Br_4)^{3-}\cdot V$. We used the theoretical values of A_{iso} and b for ^{35}Cl, quoted in table G4 of reference [30], because this nuclide has three times the natural abundance of ^{37}Cl. Only the sign combination with both $A_\parallel$ and $A_\perp$ positive gives a total spin population that is positive and less than unity. The resultant orbital-population parameters are $\sigma_s = 0.009$ and $\sigma_p = 0.197$, indicating that about 20% of the trapped hole is localized on each chloride ion.

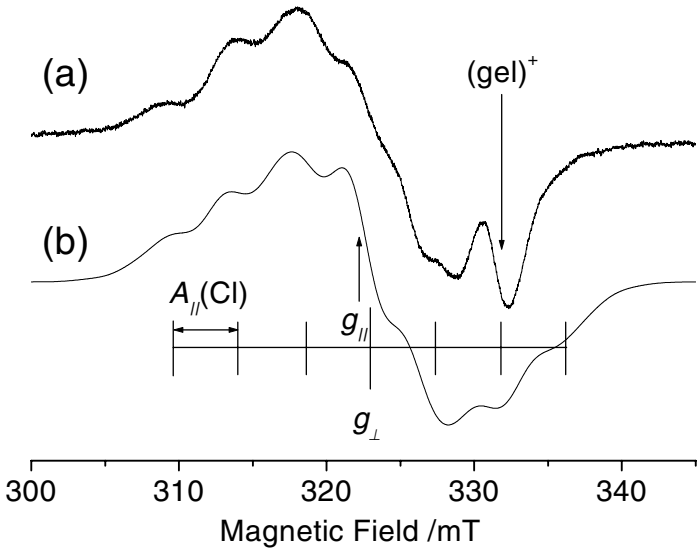

Figure 11. 9.3 GHz EPR spectra (a) measured at 10 K from a 0.06 μm AgCl cubic dispersion in gelatin following its exposure to 365 nm radiation at 10 K and dark annealing to 140 K and (b) a simulation (see the text for details).

The increased hole density on halide on going from $(Br_4)^{3-}\cdot V$ to $(Cl_4)^{3-}\cdot V$ is counter-intuitive, using arguments based on the higher electron affinity of chlorine. The results of DFT calculations are also inconsistent with the conclusions of the HF analysis. From the Mulliken analysis, only 12.4% of the hole resides on each of the four Cl^- ions adjacent to the cation vacancy. At least 7.7% is delocalized onto each of the four nearest-neighbour Ag^+ ions in the AgCl surface, and 2.2% resides on each of the eight Cl^- ions in the penultimate lattice

plane. Thus, the precise structure and composition of this high-temperature hole centre on the surface of AgCl grains remains an open question. While an assignment to $(Cl_4)^{3-}\cdot V$ seems improbable, it does appear to contain four equivalent Cl^- ions. Further EMR experiments are planned to address this issue.

5. Summary

The reactivity of photo-generated hole centres in AgBr and AgCl dispersions, as determined by multifrequency EPR spectroscopy, ENDOR spectroscopy and calculations of structure and energy, are summarized in scheme 5.

Scheme 5.

AgBr

$$h\nu \rightarrow [(Br_4)^{3-}\cdot V]_{surface} \rightarrow (i_{Br}) \rightarrow (gel)^+$$

AgCl

$$h\nu \rightarrow [(AgCl_6)^{4-}\cdot V]_{internal} \rightarrow [(AgCl_6)^{4-}]_{mobile} \rightarrow [(AgCl_6)^{4-}]_{surface} \rightarrow [(Cl_4)^{3-}]_{surface} \downarrow (i_{Cl}) \downarrow (gel)^+$$

Note that $[(Br_4)^{3-}\cdot V]_{surface}$ is formed directly at 10 K, consistent with the high hole mobility in AgBr at low temperatures [11], but there are several Ag^{2+} centres intermediate in the production of the surface $(Cl_4)^{3-}$-like acceptor. The identities of the species labelled i_{Br} and i_{Cl} are still unknown, but i_{Br} is paramagnetic. This precludes its assignment as molecular bromine. The possibility that i_{Br} and i_{Cl} are halogen atoms cannot be discounted. They oxidize gelatin to form $(gel)^+$. In the absence of gelatin, the atoms must diffuse at the grain's surface and coalesce to form molecular halogen, the evolution of which was reported in references [16] and [21].

Acknowledgments

We wish to thank S M Finn, E K Lelental, A Mickys, and J L Mount for preparing the silver halide dispersions used in these experiments. Dr A P Marchetti first suggested the use of PVA as a peptizer, and Dr M T Olm made numerous helpful suggestions during the course of this work.

References

[1] Brescia J Z, Eachus R S, Janes R and Olm M T 1987 *Cryst. Latt. Defects Amorph. Mater.* **17** 165
[2] Eachus R S and Olm M T 1989 *Cryst. Latt. Defects Amorph. Mater.* **18** 297
[3] Eachus R S and Olm M T 1991 *J. Soc. Photogr. Sci. Technol. Japan* **54** 294
[4] Pawlik Th D, Eachus R S, McDugle W G and Baetzold R C 1998 *J. Phys.: Condens. Matter* **10** 11 795
[5] Hayes W 1983 *Semicond. Insul.* **5** 533 and references therein
[6] Marchetti A P, Burberry M S and Spoonhower J P 1991 *Phys. Rev.* B **43** 2378 and references therein
[7] Olm M T, Eachus R S and McDugle W G 1993 *Bulg. Chem. Commun.* **26** 350
[8] Bennebroek M T, Poluektov O G, Zakrzewski A J, Baranov P G and Schmidt J 1995 *Phys. Rev. Lett.* **74** 442

[9] Bennebroek M T, Poluektov O G, Schmidt J, Eachus R S and Olm M T 1997 *J. Phys.: Condens. Matter* **9** 3227
[10] Eachus R S and Olm M T 1986 *Annu. Rep. Prog. Chem.* C **83** 3
[11] Marchetti A P and Eachus R S 1992 *Advances in Photochemistry* vol 17, ed D Volman D, G Hammond and D Neckers (New York: Wiley) pp 145–216
[12] Eachus R S, Marchetti A P and Muenter A A 1999 *Annu. Rev. Phys. Chem.* **50** 117
[13] Tani T 1995 *Photographic Sensitivity: Theory and Mechanisms* (Oxford: Oxford University Press)
[14] Platikanova V and Malinowski J 1978 *Phys. Status Solidi* a **47** 683
[15] Kanzaki H and Mori T 1984 *Phys. Rev.* B **29** 3573
[16] Kanzaki H and Mori T 1983 *Semicond. Insul.* **5** 401
[17] Höhne M and Stasiw M 1968 *Phys. Status Solidi* **25** K55
Höhne M and Stasiw M 1968 *Phys. Status Solidi* **28** 247
[18] For example, see Eachus R S, Pawlik Th D, Baetzold R C, Crosby D A and McDugle W G 2000 *J. Phys.: Condens. Matter* **12** 2535
[19] Spaeth J-R and Rowan L 1996 private communication
[20] Paul W B, Goldenberg S, Rowan L and Slifkin L 1987 *Cryst. Latt. Defects Amorph. Mater.* **15** 197
[21] Luckey G W 1953 *J. Phys. Chem.* **57** 791
Luckey G W 1955 *J. Chem. Phys*. **23** 882
[22] Eachus R S, Baetzold R C, Pawlik Th D, Poluektov O G and Schmidt J 1999 *Phys. Rev.* B **59** 8560
[23] Berry C R 1977 *The Theory of the Photographic Process* ed T H James (New York: Macmillan) ch 3
[24] Pawlik Th D, Eachus R S, Baetzold R C and McDugle W G 2000 *J. Phys.: Condens. Matter* **12** 2555
[25] McGavin D G, Mombourquette M J and Weil J A 1993 *Computer Program EPR-FOR* version 5.1, Department of Chemistry, University of Saskatchewan
[26] Hyde J S, Rist G H and Erikson L E 1968 *J. Phys. Chem.* **72** 4269
[27] Feher G 1959 *Phys. Rev.* **114** 1219
[28] Spaeth J-M, Niklas J R and Bartram R H 1992 *Structural Analysis of Point Defects in Solids* (Berlin: Springer)
[29] Castner T G and Känzig W 1957 *Phys. Chem. Solids* **178** 3
[30] Weil J A, Bolton J R and Werz J E 1994 *Electron Paramagnetic Resonance* (New York: Wiley)
[31] Baetzold R C 1997 *J. Phys. Chem.* B **101** 8180
[32] Hay P J and Wadt W R 1985 *J. Chem. Phys.* **82** 270
[33] Wadt W R and Hay P J 1985 *J. Chem. Phys.* **82** 284